Langmuir

Article

pubs.acs.org/Langmuir

Nonvolatile Memory Devices Prepared from Sol–Gel Derived Niobium Pentoxide Films

Hyunhee Baek,[†,§] Chanwoo Lee,[‡,§] Jungkyu Choi,*[,†] and Jinhan Cho*[,†]

[†]Department of Chemical & Biological Engineering, Korea University, Anam-dong, Seongbuk-gu, Seoul 136-713, South Korea

[‡]School of Advanced Materials Engineering, Kookmin University, Jeongneung-dong, Seongbuk-gu, Seoul 136-702, South Korea

Supporting Information

ABSTRACT: We report on the resistive switching nonvolatile memory (RSNM) properties of niobium pentoxide (Nb_2O_5) films prepared using sol–gel chemistry. A sol–gel derived solution of niobium ethoxide, a precursor to Nb_2O_5, was spin-coated on to a platinum (Pt)-coated silicon substrate, and was then annealed at approximately 620 and 450 °C to form a Nb_2O_5 film of polycrystalline and amorphous structure, respectively. A top electrode consisting of Ag, W, Au, or Pt was then coated onto the Nb_2O_5 films to complete the fabrication. After a forming process of limited current compliance up to 10 mA, known as "electroforming", a resistive switching phenomenon, independent of voltage polarity (unipolar switching), was observed at low operating voltages (0.59 ± 0.05 V_{RESET} and 1.03 ± 0.06 V_{SET}) with a high ON/OFF current ratio above 10^8. The reported approach offers opportunities for preparing Nb_2O_5-based resistive switching memory devices from solution process.

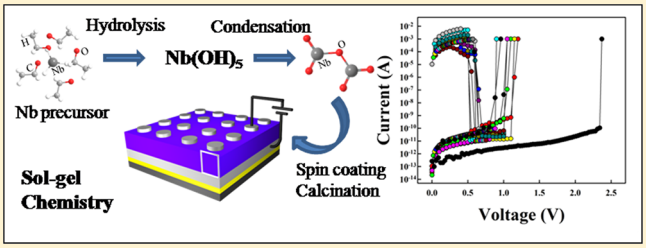

INTRODUCTION

Resistive switching nonvolatile memory (RSNM) devices have attracted considerable attention in the field of mobile electronics because of their excellent memory performance (e.g., ON/OFF current ratio of 10^3 to 10^6, fast switching speeds, and low operating voltage).[1−19] Transition metal oxides such as TiO_2, NiO, ZrO, and $SrTiO_x$ prepared by vacuum deposition have been widely used as resistive switching materials for nonvolatile memory devices. These transition metal oxide films have excellent thermal stability and operating durability in air. Recently, much effort has been put into the preparation of RSNM films based on solution process to produce large-area devices at low cost by a simplified manufacturing process in a timely manner. For example, soluble polymers have been recognized as notable candidates for the active layers in next-generation nonvolatile memory devices, because they can be deposited using facile solution processes, such as spin-coating or layer-by-layer assembly.[14,15,20−22] However, these organic memory devices have much difficulty in sufficiently securing the high memory performance and the excellent environmental stability shown in transition metal oxide-based devices. Therefore, many research groups have focused on the preparation of RSNM devices, with excellent memory performance and stability, through solution processes. Although perovskite oxide (e.g., $La_{1-x}Ca_xMnO_3$,[11] and $SrZrO_3$[12])-based RSNM devices can be prepared by a sol–gel solution process and subsequent thermal annealing instead of vacuum deposition, the perovskite materials with multications contain chemical compositions which are more complex than those of the binary transition metal oxides, such as TiO_2 or Nb_2O_5. Perovskite oxide-based devices have also exhibited a low ON/OFF current ratio less than 10^3. Recently, it was reported that TiO_2 RSNM devices prepared by a sol–gel solution process exhibited resistive switching characteristics with an ON/OFF current ratio of about 10^5.[9] Furthermore, in our previous study, we suggested the possibility that sol–gel derived Nb_2O_5 film with an amorphous structure could display the resistive switching memory property.[9]

Herein, we systematically investigate the memory characteristics of sol–gel derived Nb_2O_5 films with polycrystalline and amorphous structure, in terms of their chemical composition and memory performance. Additionally, these film devices exhibited a memory performance with high ON/OFF current ratio greater than 10^8, a rapid switching speed (nanoseconds), and low operating voltages less than 1.5 V. Although niobium oxide (NbO_2)-based RSNM devices were reported by one research group,[23] they were mainly prepared by the vacuum deposition method, and furthermore, exhibited relatively low ON/OFF current ratios of about 10^2 to 10^4, compared to that of our sol–gel-based devices. For this study, niobium ethoxide was used as a precursor of niobium pentoxide (Nb_2O_5) for the resistive switching material, which could be converted into Nb_2O_5 with an oxygen deficiency state after controlled-thermal annealing. In this case, the sol–gel derived Nb_2O_5 introduced no additional components, such as dopants or metal nanoparticles. Considering that the sol–gel Nb_2O_5 film devices exhibit excellent memory performance, we believe that sol–gel

Received: May 31, 2012
Revised: November 24, 2012
Published: December 4, 2012

derived Nb_2O_5 films can be used as electrically active films for resistive switching nonvolatile memory devices with a solution-based manufacturing process.

EXPERIMENTAL SECTION

Preparation of Nb_2O_5 Films from Niobium Precursor. One gram of niobium ethoxide (e.g., $Nb(OCH_2CH_3)_5$) (Aldrich, 97%) was dissolved in 10 g of isopropyl alcohol (IPA 99.9%). The mixed solution was hydrolyzed according to a reference procedure, by adding 0.07 g of HCl dropwise.[25] These solutions were spin-coated onto Pt electrode-coated SiO_2 substrates at 4000 rpm. The resulting films were thermally annealed at 620 °C for 2 h under a nitrogen atmosphere, and were further annealed at 620 °C for 4 h in oxygen to form Nb_2O_5.

Surface Morphology. The surface morphology and roughness of thermally annealed Nb_2O_5 films onto Si substrates were investigated by atomic force microscopy (AFM) in tapping mode (XE-100, Parksystem).

X-ray Diffraction (XRD) Measurement. Crystal structures of sol–gel derived Nb_2O_5 films were examined using X-ray diffraction (XRD) at room temperature. Data collection was performed in the 2θ range from 15° to 60° using Cu Kα radiation (λ = 1.54 Å, model: Bruker D8 Discover, Germany). Cross-sectional TEM (model: JEOL 300 kV) was also used to examine the Nb_2O_5 crystal structure and internal structure of the nanocomposite multilayers.

X-ray Photoelectron Spectroscopy (XPS) Measurement. XPS spectra for the binding state of Nb ions were obtained using an AXIS-His spectrometer with monochromatic Mg Kα radiation (1253.6 eV). The survey spectra were recorded in the range 0–1200 eV with a constant pass energy of 20 eV; the high-resolution spectra were recorded with a constant pass energy of 20 eV. The X-ray source was run at a reduced power of 150 W. The pressure in the analysis chamber was maintained at 5×10^{-9} Pa for measurement. The Ar ion milling for Nb_2O_5 films was not used for XPS measurement because it could generate the various Nb suboxide peaks by the reduction of niobium pentoxide.

Fourier Transform Infrared (FT-IR) Spectroscopy. Vibrational spectroscopic characterization was carried out using FTIR spectroscopy (spectrum 400, Perkin-Elmer) in the transmission. Sample chamber was purged with N_2 gas for 2 h to eliminate water and CO_2 before FTIR measurement.

Material Component Analysis. Impurity analyses were carried out using HR-TEM (Tecnai G2 F20, Philips, The Netherlands) images, EF-TEM (energy-filtered transmission electron microscopy) maps, and EDS (energy dispersive X-ray spectroscopy). The cross-sectional TEM specimens were prepared using a focused ion beam (FIB, SEIKO, SMI3050, Japan) etching technique. The oxygen composition gradient was investigated using TEM-EDS line analysis on cross-sectional areas of treated samples (see Supporting Information, Figure S1).

Fabrication of RSNM Devices. All samples were prepared on Si substrates with a 100-nm-thick SiO_2 layer. A 20-nm-thick Ti layer was then deposited on the SiO_2 layers followed by a 100-nm-thick bottom electrode (Pt), by DC-magnetron sputtering. In this case, the Ti layer was used to improve the adhesion between the SiO_2 and Pt bottom electrode. Sol–gel derived Nb_2O_5 films were then deposited on the Pt-coated Si substrates using a spin-coating method with a spin speed of 4000 rpm. The resulting multilayer films were thermally annealed at 620 °C for 2 h under a nitrogen atmosphere, followed by further annealing at the same temperature for 4 h in oxygen. After thermal conversion, 100-μm-diameter Ag top electrodes were deposited on the nanocomposite films. The resistive switching behavior of the sol–gel derived Nb_2O_5 devices were examined by measuring the current–voltage (I–V) curves using a semiconductor parametric analyzer (SPA, Agilent 4155B) in air. The pulsed voltage duration dependence of the high and low current states was investigated using a semiconductor parametric analyzer (HP 4155B) and pulse generator (Agilent 8110A). In addition, local current maps on the scale of nanometers were measured using current sensing atomic force microscopy (CS-AFM) (XE-100, Park system) in contact mode with conducting tips. We determined the electrical switching properties of about 100 samples, and consequently obtained satisfactory switching results, with about 70% yield in laboratory environments (see Supporting Information, Figure S2).

RESULTS AND DISCUSSION

Sol–gel processing was performed on a Nb_2O_5 precursor solution by a hydrolysis and condensation reaction with hydrochloric acid. The sol–gel derived solution was thermally annealed—first in nitrogen at 620 °C and then in air at 620 °C to form a Nb_2O_5 film. The initial thermal annealing process in nitrogen can induce oxygen vacancies accompanied by an increase in local electron concentration.[9,24] Below 600 °C, residual carboxylate or carbonate groups are known to prevent crystallization. Narendar and Messing (1997) reported that the crystallization of a Nb_2O_5 film occurs at temperatures higher than 580 °C because of the complete thermal decomposition of residual organic groups.[26] Due to the thermal degradation of organic material, these films showed a weight loss of approximately 23% (see Supporting Information, Figure S3), while the decomposition of residual carboxylate or carbonate groups in the range of 580 to 600 °C accounted for approximately 4% of the weight loss. As confirmed by cross-sectional scanning electron microscopy (SEM) (Figure 1), the

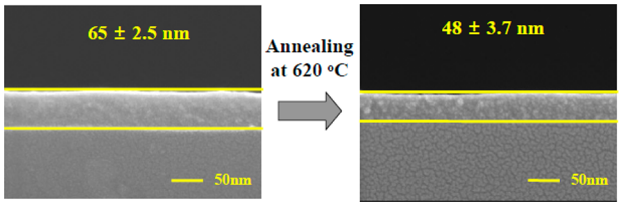

Figure 1. Cross-sectional SEM images of niobium ethoxide and thermally annealed Nb_2O_5 films.

thickness of the Nb_2O_5 film (48 ± 3 nm) was reduced to approximately 74% of the initial film thickness prior to annealing (65 ± 2 nm). The root-mean-square (RMS) surface roughness of the films was determined to be approximately 2.7 nm in the 1.0 × 1.0 μm^2 area (see Supporting Information, Figure S4).

XRD and cross-sectional HR-TEM were used to examine the formation of the Nb_2O_5 film and crystalline structure after annealing. The (001) and (100) peaks from the Nb_2O_5 film formed by the sol–gel process and thermal annealing were clearly observed by XRD (Figure 2a), while the formation of (001) and (100) Nb_2O_5 was confirmed by HR-TEM.[27] The lattice spacing was determined to be 3.93 and 3.12 Å, respectively (Figure 2b). Because the initial thermal annealing process in nitrogen could have increased the local electron concentration by inducing oxygen deficiencies, the chemical compositions of Nb_2O_5 films were analyzed by X-ray photoelectron spectroscopy (XPS) (Figure 2c,d). As shown in Figure 2c, the Nb $3d_{3/2}$ and $3d_{5/2}$ XPS peaks were resolved into two spin–orbit components, assigned as Nb^{5+} (207 eV) and Nb^{4+} (206.6 eV).[28] The presence of the Nb^{4+} peak indicates the generation of oxygen vacancies within the films. The Nb^{4+}/Nb^{5+} ratio was approximately 0.22, and additionally, the sol–gel derived Nb_2O_5 films were nonstoichiometric with the composition ratio of Nb/O = 2:4.16. We did not detect the residual carbons within Nb_2O_5 film devices (see Supporting Information, Figure S5). Furthermore, we investigated the presence of residual hydrogens within sol–gel derived Nb_2O_5

dx.doi.org/10.1021/la303857b | Langmuir 2013, 29, 380–386

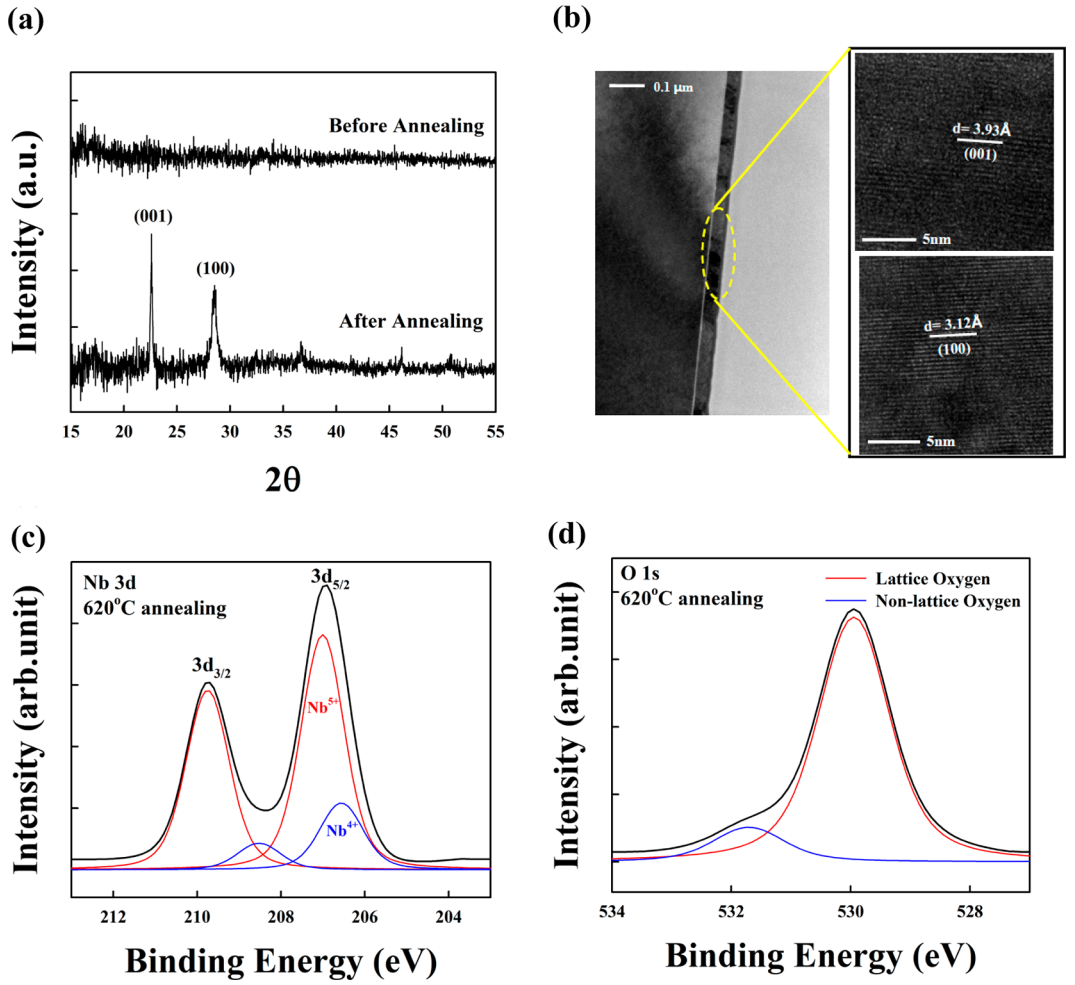

Figure 2. (a) XRD patterns of niobium ethoxide and thermally annealed Nb_2O_5 films at 620 °C. (b) Cross-sectional HR-TEM image of Nb_2O_5 films. XPS spectra and deconvoluted spectra of (c) Nb 3d and (d) O 1s of Nb_2O_5 films.

film using FT-IR spectroscopy. In the case of Nb_2O_5 films thermally annealed at 450 and 620 °C, the peaks at 600 and 900 cm^{-1} are assigned to the stretching vibration of Nb−O and Nb−O−Nb bonds, respectively (see Supporting Information, Figure S6).[29,30] On the other hand, the absorption peaks centered around 3400 and 1630 cm^{-1} are associated with the adsorbed water and hydroxyl groups onto the surface of Nb_2O_5 films.[29] On the basis of these results, we could not confirm the presence of residual hydrogens, possibly contributing to the switching, within the films.

It was reported that Nb_2O_5[31] and NbO_2[32] have insulating and n-type semiconducting properties, respectively. Therefore, it is expected that the presence of Nb^{4+} within sol−gel derived Nb_2O_5 films may act as n-type dopants, which can transform an insulating oxide into a semiconductor. It was previously reported that an applied electric field can cause the injection of electrons into the conduction band of transition metal oxides, followed by reduction to metastable oxygen vacancies.[4,33] This suggests that Nb_2O_5 films fabricated by a sol−gel process can be used as efficient active layers in RSNM devices.

On the basis of these results, resistive switching memory devices composed of Pt bottom electrode, the sol−gel derived Nb_2O_5 films, and top electrodes (i.e., electrochemically active Ag, electrochemically inert W, Au, and Pt) were fabricated (Scheme 1). These various top electrodes were employed for investigating the effect of electrochemically active and inert

Scheme 1. Schematic for RSNM Devices Based on Sol−Gel Derived Nb_2O_5 Films

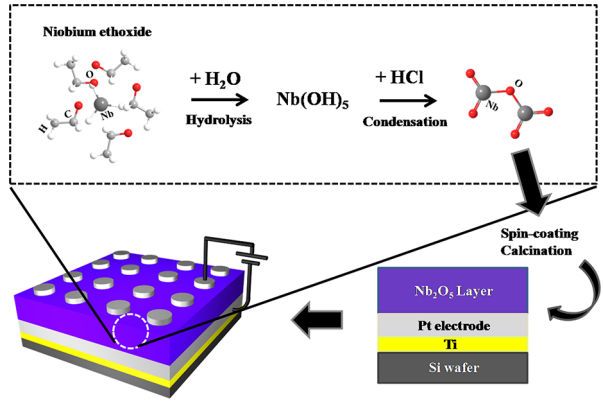

electrodes on the device performance. All the bias was applied with respect to the top electrodes, while the bottom electrode was grounded.

During the first applied positive voltage sweep, a sharp increase in current from the device with Ag top electrodes (100 μm in diameter) occurred at approximately 2.2 V. In the forming process of limited current compliance up to 0.1 mA, known as "electroforming", a certain electrical field should be reached in order to generate highly defective components and

dx.doi.org/10.1021/la303857b | Langmuir 2013, 29, 380−386

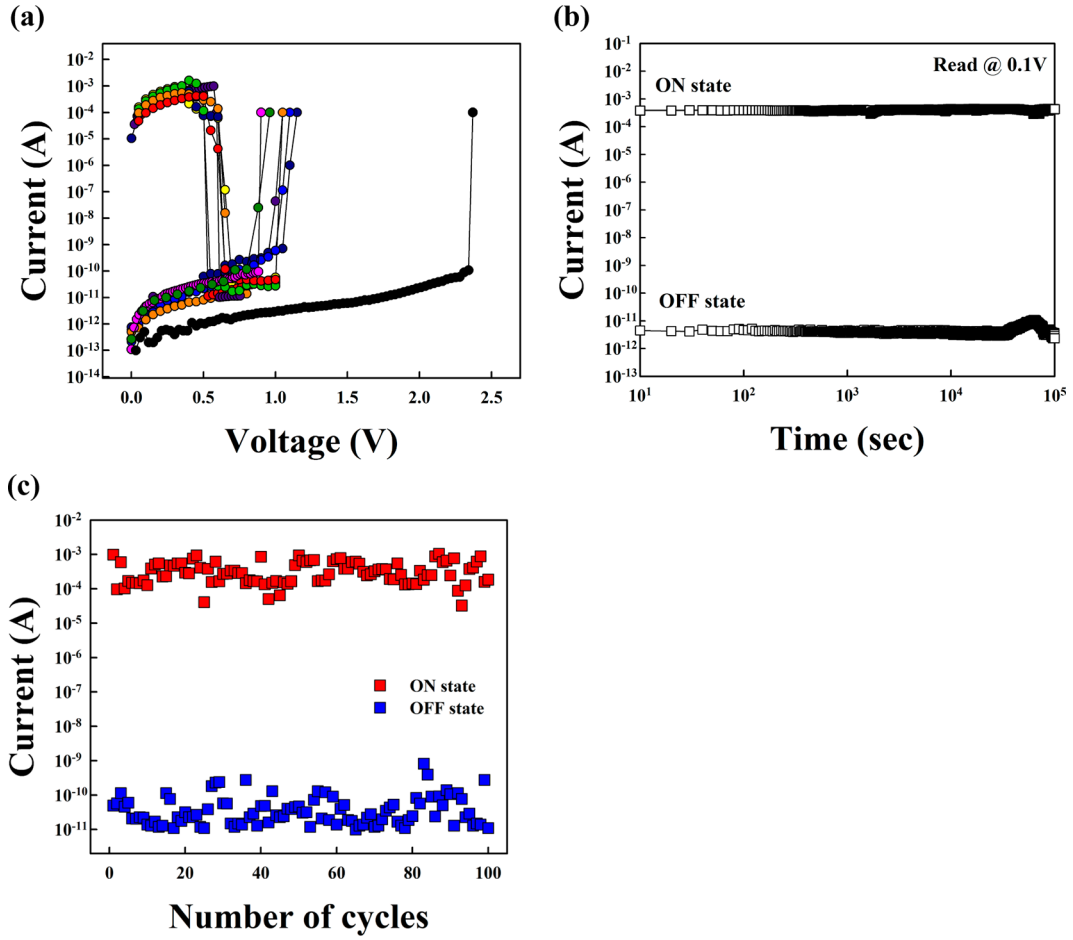

Figure 3. (a) Repeated $I-V$ curves and (b) retention time test of sol–gel derived Nb_2O_5 devices measured from a switching speed of 600 μs. (c) Cycling test of Nb_2O_5 devices measured from a switching speed of 100 ns.

to create conducting filamentary paths connecting the two electrodes. Hence, the electroforming voltage becomes higher for the thicker metal oxide films (see Supporting Information, Figure S7). The high current state (ON state) that formed after the electroforming process returned to the low current state (OFF state) with an abrupt decrease in current at 0.59 ± 0.05 V (i.e., RESET voltage, V_{RESET}) during the second voltage sweep (from the ON state to the OFF state, or from 0 to 1.0 ± 0.2 V) with limited current compliance up to 10 mA. When voltage applied to the device was increased again, a sharp increase in current was observed at 1.03 ± 0.06 V (i.e., SET voltage, V_{SET}). In addition, an ON/OFF current ratio between the high and low current states was measured to be approximately ~10^8 (Figure 3a). This switching phenomenon, known as "unipolar switching behavior", which does not depend on the polarity of the applied voltage to form the high and low current states,[2] is caused by the formation and disruption of conducting filamentary paths within these oxide layers. V_{RESET} and V_{SET} of the conventional devices prepared by vacuum deposition are generally above 1 and 2 V, respectively.[23] Compared to these conventional devices prepared from vacuum deposition process, the present devices have been shown to operate with lower electroforming and operating voltages. Although not fully understood, these phenomena are mainly caused by the formation of relatively many material-based defects (oxygen deficiencies, grain boundaries, or dislocations) within the sol–gel derived Nb_2O_5 films, compared to those within the vacuum-deposited metal oxide films.[34−39] These phenomena were also observed from the sol–gel derived TiO_2 film devices as previously reported by our group.[9] That is, the thermal conversion of organometallic components in an oxygen-deficient environment (i.e., a nitrogen atmosphere) can produce a number of material-based defects that are very favorable to the formation of conductive filaments.

A cycling test was carried out in manual mode using a switching speed of 600 μs and a reading voltage of 0.1 V to determine the electrical stability of the sol–gel Nb_2O_5 devices in the ON and OFF states. In this case, the ON and OFF states were observed to be stable during the repeated cycling tests, maintaining a high ON/OFF current ratio of ~10^8 (see Supporting Information, Figure S8). To further demonstrate the stability of the resistive switching properties, data retention was gauged by examining the current level of the device in the ON state in ambient air over a long period of time (>10^5 s). In this case, no appreciable change in conductivity was observed in these devices, as shown in Figure 3b. It was also observed that Nb_2O_5-based devices could be repeatedly operated at a switching speed of 100 ns (Figure 3c). In this case, a reading voltage of 0.1 V was used for the measurement of current states. The resistive switching curves of devices measured after one year was almost similar to those of the initial film device (i.e., device measured before one year), demonstrating the fast switching speed, as well as the excellent electrical and environmental stability of the devices (see Supporting

dx.doi.org/10.1021/la303857b | *Langmuir* 2013, 29, 380−386

Information, Figure S9). It was reported that solid electrolytes sandwiched between a Ag (or Cu) and inert electrodes could display resistive switching behavior as a result of an electrochemical redox reaction from the high mobility of Ag ions.[7,40,41] However, a similar switching behavior with low operating voltages below 1.5 V and high ON/OFF current ratio of above $\sim 10^5$ was also observed from electrochemically inert W, Au, and Pt electrodes with a diameter of 100 μm (see Supporting Information, Figure S10), indicating that the Ag electrode itself has no significant effect on the resistive switching characteristics of sol–gel derived Nb_2O_5.

During the repetitive switching cycles, local current images were monitored by current-sensing atomic force microscopy (CS-AFM) to determine the extent of reversibility between the formation and disruption of the conducting filamentary paths within the sol–gel derived Nb_2O_5 films. In these measurements, the CS-AFM tip (i.e., electrochemically inert Pt tip) was used instead of Ag as the top electrode. Bright regions in the CS-AFM images, as shown in Figure 4, indicate the occurrence

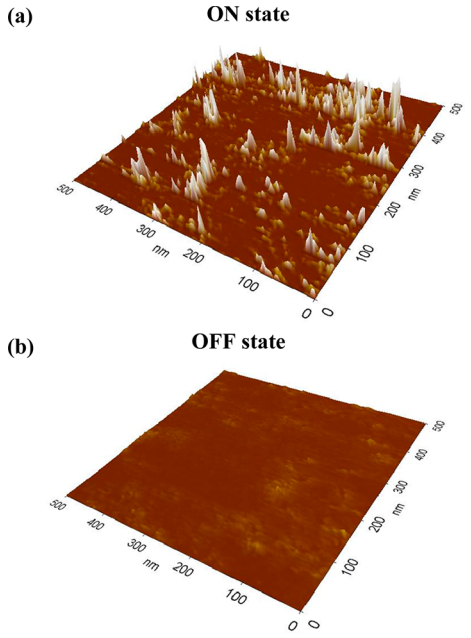

Figure 4. CS-AFM images of Nb_2O_5 film device in ON (~4 V) and OFF (~1.5 V) state, respectively. The Pt tip used as a top electrode has an electrical point source with a small contact area of about 50 nm.

of conductive filamentary paths. At electroforming voltages between 1 and 7 V, localized conductive paths were formed randomly; at 10 V, the reversible switching properties of the films were lost as a result of dielectric breakdown (see Supporting Information, Figure S11).

On the basis of these electrical properties, the voltages for device operation for the ON and OFF states were adjusted on the nanometer scale. As shown in Figure 4, the formation and rupture of randomly distributed paths were observed after the SET and RESET processes, which show that the current densities between the top and bottom electrodes were not uniform, but were concentrated in localized conductive paths that were turned on and off during switching. In addition, operating voltages for the OFF (i.e., 1.2 V) and ON (i.e., 3.8 V) states were higher than those from the devices shown in Figure 3a.

One possible explanation for the increased voltage thresholds of the SET and RESET processes may be that there is an additional energy barrier from interfacial surface contamination on conducting CS-AFM tip surfaces. It is also possible that the CS-AFM tip, because of its small contact area (~50 nm), can operate as an electrical point source, thereby causing the electric field exerted from the tip throughout the Nb_2O_5 films to be nonuniform. A nonuniform electric field is known to increase the applied voltages for resistive switching.[9,15] Another possibility is that the decrease of material-based defects in a small cell area can significantly increase the operation voltages. As mentioned earlier, the material based defects such as grain boundaries and dislocations provide easy diffusion paths for oxygen vacancies in the metallic oxides, and as a result, conducting paths are apt to form at grain boundaries. Therefore, a decrease of cell area reduces the density of conductive filamentary paths formed under a top electrode, and consequently increases high operating voltages. In order to confirm this possibility, the operating voltages of polycrystalline Nb_2O_5 film devices were also investigated using three different sizes of top electrodes (i.e., 50-nm-sized AFM Pt tip electrode, 30-μm- and 100-μm-sized Pt electrodes). In this case, the operating voltages were increased by decreasing the size of the top electrode (see Supporting Information, Figure S12). The unipolar switching behavior observed in these devices can be described as a conducting filamentary model of fuse–antifuse type as mentioned earlier.[1,17,42−44] Once the conducting filamentary paths are formed, the current flow concentrates on these local paths and the conducting paths grow very fast due to local heating by the concentrated current flow (i.e., switching from low conductivity to high conductivity states). The destruction of the filamentary paths (i.e., switching from high conductivity to low conductivity states) is believed to be accompanied by thermal rupture of the filaments (i.e., by the heat produced from the large current flow). For confirming conductive filamentary model based on Joule heating, we investigated the dependences of resistance characteristics on the cell area for low resistance state (LRS) and high resistance state (HRS). Although there was no obvious dependence of the LRS on the electrode size for conductive filament formation after SET process, the resistance at HRS decreased with increasing the cell size. The lower resistance of large-sized cells results in a higher RESET current at the same applied voltage bias. As a result, a higher RESET current generates enough Joule heat to break large amounts of conductive filaments (see Supporting Information, Figure S13).

Although our devices were prepared with polycrystalline Nb_2O_5 films annealed at a high temperature of 620 °C, the amorphous Nb_2O_5 films annealed at 450 °C also exhibited memory performance with an ON/OFF current ratio of $\sim 10^7$ (see Supporting Information, Figure S14). A low-temperature process is more desirable for complementary metal-oxide-semiconductor (CMOS) technologies. However, it was found that electroforming (~2.6 V) /operating voltages (V_{RESET} ~ 0.61 ± 0.08 V and V_{SET} ~ 1.71 ± 0.19 V) were increased relatively compared to those measured from polycrystalline Nb_2O_5 films (Figure 3a). In this case, the composition ratio of Nb and O (or Nb^{4+}/Nb^{5+} ~ 0.16) in the amorphous Nb_2O_5 films was determined to be about 2:4.34, which showed relatively low oxygen deficiencies compared to that of polycrystalline Nb_2O_5 (Nb/O = 2:4.16 and Nb^{4+}/Nb^{5+} ~ 0.22) (see Supporting Information, Figure S15). Although it has been reported that a high degree of crystallinity provided

dx.doi.org/10.1021/la303857b | *Langmuir* 2013, 29, 380–386

fewer sites for conduction path formation, and as a result caused higher electroforming and operating voltages,[45,46] the polycrystalline Nb_2O_5 films thermally converted from an organometallic precursor at 620 °C can significantly increase the density of available sites (i.e., grain boundaries and dislocations) for the formation of conduction paths composed of relatively many oxygen vacancies, compared to the amorphous Nb_2O_5 films annealed at 450 °C.

On the other hand, the use of electrochemically inert W, Au, and Pt electrodes instead of Ag top electrodes had no significant effect on electroforming and operating voltages (see Supporting Information, Figure S10). These results imply that the low electroforming and SET voltages shown in the polycrystalline Nb_2O_5 films are strongly dependent on the material-based defects. Although it has been recently reported that the switching properties of nonvolatile memory devices composed of SiO_2/Ti (5 nm)/Pt (15 nm)/TiO_{2-x} (40 nm)/Pt (30 nm) annealed at 250 °C can be significantly improved by the diffusion of Ti-reactive metal atoms, through the contact bottom electrodes to the TiO_{2-x} switching layer,[47] the diffusion of the thermally diffused Ti layer into the switching metal oxide layer was not observed in our devices (see Supporting Information, Figure S16). Furthermore, sol–gel derived Nb_2O_5 film devices without Ti layer also exhibited the resistive switching behavior similar to that with Ti Layer (see Supporting Information, Figure S17).

As a result, the material-based defects such as oxygen deficiencies, grain boundaries, and dislocations instead of thermal diffusion of Ti adhesion layer have a significant effect on the formation of local conducting filamentary paths at low electroforming and operating voltages.

CONCLUSIONS

We have demonstrated that Nb_2O_5 prepared by a facile sol–gel method can be used effectively in the fabrication of unipolar switching memory devices with low operating voltages (V_{RESET} ~ 0.59 V ± 0.05 and V_{SET} ~ 1.03 ± 0.06), fast switching speed, high ON/OFF current ratio of ~10^8, and electrical stability. This switching mechanism could be explained by a conducting filamentary model. Furthermore, we also showed that the memory performance of sol–gel Nb_2O_5 devices was not significantly dependent on crystallinity or the electrochemical activity of top electrodes. The sol–gel derived Nb_2O_5 films can contribute to the production of RSNM devices with large ON/OFF current ratio, allowing solution process.

ASSOCIATED CONTENT

Supporting Information

Depth-distribution profile, TEM-EDS data, TGA data, AFM image, EDS data, FT-IR spectra, electroforming voltage data, cycling tests, *I*–*V* curves, CS-AFM images, cell size dependence, XPS spectra, and EF-TEM of sol–gel derived Nb_2O_5 films. This material is available free of charge via the Internet at http://pubs.acs.org.

AUTHOR INFORMATION

Corresponding Author

*E-mail: jinhan71@korea.ac.kr; jungkyu_choi@korea.ac.kr.

Author Contributions

§These authors contributed equally to this work.

Notes

The authors declare no competing financial interest.

ACKNOWLEDGMENTS

This work was supported by the National Research Foundation (NRF) grant funded by the Korea government (MEST) (2010-0029106) and ERC Program of NRF grant funded by the Korea government (MEST) (R11-2005-048-00000-0) (Prof. Cho). This work was also supported by a Korea University Grant (Prof. Choi).

REFERENCES

(1) Waser, R.; Aono, M. Nanoionics-based resistive switching memories. *Nat. Mater.* **2007**, *6*, 833.

(2) Szot, K.; Speier, W.; Bihlmayer, G.; Waser, R. Switching the electrical resistance of individual dislocations in single-crystalline $SrTiO_3$. *Nat. Mater.* **2006**, *5*, 312.

(3) Strukov, D. B.; Snider, G. S.; Stewart, D. R.; Williams, R. S. The missing memristor found. *Nature* **2008**, *453*, 80.

(4) Yang, J. J.; Pickett, M. D.; Li, X.; Ohlberg, D. A. A.; Stewart, D. R.; Williams, R. S. Memristive switching mechanism for metal/oxide/metal nanodevices. *Nat. Nanotechnol.* **2008**, *3*, 429.

(5) Oka, K.; Yanagida, T.; Nagashima, K.; Kawai, T.; Kim, J.-S.; Park, B. H. Resistive-switching memory effects of NiO nanowire/metal junctions. *J. Am. Chem. Soc.* **2010**, *132*, 6634.

(6) Rozenberg, M. J.; Inoue, I. H.; Sánchez, M. J. Strong electron correlation effects in nonvolatile electronic memory devices. *Appl. Phys. Lett.* **2006**, *88*, 033510.

(7) Kozicki, M. N.; Yun, M.; Hilt, L.; Singh, A. *The Electrochemical Society Proceedings Series*; Electrochemical Society: Pennington, NJ, 1999; p 298.

(8) Lee, M. J.; Lee, C. B.; Lee, D.; Lee, S. R.; Chang, M.; Hur, J. H.; Kim, Y. B.; Kim, C. J.; Seo, D. H.; Seo, S.; Chung, U. I.; Yoo, I. K.; Kim, K. A Fast, High-endurance and scalable non-volatile memory device made from asymmetric Ta_2O_{5-x}/TaO_{2-x} bilayer structures. *Nat. Mater.* **2011**, *10*, 625.

(9) Lee, C.; Kim, I.; Choi, W.; Shin, H.; Cho, J. Resistive switching memory devices composed of binary transition metal oxides using sol-gel chemistry. *Langmuir* **2009**, *25*, 4274.

(10) Qi, J.; Olmedo, M.; Ren, J.; Zhan, N.; Zheng, J.-G.; Liu, J. Resistive switching in single epitaxial ZnO nanoislands. *ACS Nano* **2012**, *6*, 1051.

(11) Zhang, T.; Su, Z.; Chen, H.; Ding, L.; Zhang, W. Resistance switching properties of sol-gel derived $La_{0.67}Ca_{0.33}Mn_{O3}$ thin films on F-doped SnO_2 conducting glass. *Appl. Phys. Lett.* **2008**, *93*, 172104.

(12) Liu, C.-Y.; Tseng, T.-Y. Resistance switching properties of sol–gel derived $SrZrO_3$ based memory thin films. *J. Phys. D: Appl. Phys.* **2007**, *40*, 2157.

(13) Schoen, D. T.; Xie, C.; Cui, Y. Electrical switching and phase transformation in silver selenide nanowires. *J. Am. Chem. Soc.* **2007**, *129*, 4116.

(14) Kim, Y.; Lee, C.; Shim, I.; Wang, D.; Cho, J. Nucleophilic substitution reaction based layer-by-layer growth of superparamagnetic nanocomposite films with high nonvolatile memory performance. *Adv. Mater.* **2010**, *22*, 5140.

(15) Lee, C.; Kim, I.; Shin, H.; Kim, S.; Cho, J. Nonvolatile memory properties of Pt nanoparticle-embedded TiO_2 nanocomposite multilayers via electrostatic layer-by-layer assembly. *Nanotechnology* **2010**, *21*, 185704.

(16) Lee, M.-J.; Park, Y.; Suh, D.-S.; Lee, E.-H.; Seo, S.; Kim, D.-C.; Jung, R.; Kang, B.-S.; Ahn, S.-E.; Lee, C. B.; Seo, D. H.; Cha, Y.-K.; Yoo, I.-K.; Kim, J.-S.; Park, B. H. Two series oxide resistors applicable to high speed and high density nonvolatile memory. *Adv. Mater.* **2007**, *19*, 3919.

(17) Lee, J.; Bourim, E. M.; Lee, W.; Park, J.; Jo, M.; Jung, S.; Shin, J.; Hwang, H. Effect of ZrO_x/HfO_x bilayer structure on switching uniformity and reliability in nonvolatile memory applications. *Appl. Phys. Lett.* **2010**, *97*, 172105.

(18) Rohde, C.; Choi, B. J.; Jeong, D. S.; Choi, S.; Zhao, J.-S.; Hwang, C. S. Identification of a determining parameter for resistive switching of TiO_2 thin films. *Appl. Phys. Lett.* **2005**, *86*, 262907.

(19) Sawa, A.; Fujii, T.; Kawasaki, M.; Tokura, Y. Hysteretic current–voltage characteristics and resistance switching at a rectifying $Ti/Pr_{0.7}Ca_{0.3}MnO_3$ interface. *Appl. Phys. Lett.* **2004**, *85*, 4073.
(20) Koo, B.; Baek, H.; Cho, J. Control over memory performance of layer-by-layer assembled metal phthalocyanine multilayers via molecular-level manipulation. *Chem. Mater.* **2012**, *24*, 1091.
(21) Ko, Y.; Kim, Y.; Baek, H.; Cho, J. Electrically bistable properties of layer-by-layer assembled multilayers based on protein nanoparticles. *ACS Nano* **2011**, *5*, 9918.
(22) Baek, H.; Lee, C.; Park, J.; Kim, Y.; Koo, B.; Shin, H.; Wang, D.; Cho, J. Layer-by-layer assembled enzyme multilayers with adjustable memory performance and low power consumption via molecular-level control. *J. Mater. Chem.* **2012**, *22*, 4645.
(23) Jung, K.; Kim, Y.; Park, Y. S.; Jung, W.; Choi, J.; Park, B.; Kim, H.; Kim, W.; Hong, J.; Im, H. Unipolar resistive switching in insulating niobium oxide film and probing electroforming induced metallic components. *J. Appl. Phys.* **2011**, *109*, 054511.
(24) Knauth, P.; Tuller, H. L. Electrical and defect thermodynamic properties of nanocrystalline titanium dioxide. *J. Appl. Phys.* **1999**, *85*, 897.
(25) Bansal, N. P. Synthesis and thermal evolution of structure in alkoxide-derived niobium pentoxide gels. *J. Mater. Sci.* **1994**, *29*, 4481.
(26) Narendar, Y.; Messing, G. L. Synthesis, decomposition and crystallization characteristics of peroxo–citrato–niobium: an aqueous niobium precursor. *Chem. Mater.* **1997**, *9*, 580.
(27) Liu, J.; Xue, D.; Li, K. Single-crystalline nanoporous Nb_2O_5 nanotubes. *Nanoscale Res. Lett.* **2011**, *6*, 138.
(28) Özer, N.; Barreto, T.; Büyüklimanli, T.; Lampert, C. M. Characterization of sol-gel deposited niobium pentoxide films for electrochromic devices. *Sol. Energy Mater. Sol. Cells* **1995**, *36*, 433.
(29) Ge, S.; Jia, H.; Zhao, H.; Zhang, L. First observation of visible light photocatalytic activity of carbon modified Nb_2O_5 nanostructures. *J. Mater. Chem.* **2010**, *20*, 3052.
(30) Fielicke, A.; Meijer, G.; Helden, G. Infrared spectroscopy of niobium oxide cluster cations in a molecular beam: identifying the cluster structures. *J. Am. Chem. Soc.* **2003**, *125*, 3659.
(31) Jung, K.; Kim, Y.; Jung, W.; Im, H.; Park, B.; Hong, J.; Lee, J.; Park, J.; Lee, J.-K. Electrically induced conducting nanochannels in an amorphous resistive switching niobium oxide film. *Appl. Phys. Lett.* **2010**, *97*, 233509.
(32) Adler, D. Mechanisms for metal-nonmetal transitions in transition-metal oxides and sulfides. *Res. Mod. Phys.* **1968**, *40*, 714.
(33) Barman, S.; Deng, F.; McCreery, R. C. Conducting polymer memory devices based on dynamic doping. *J. Am. Chem. Soc.* **2008**, *130*, 11073.
(34) Kim, S.; Choi, Y.-K. Resistive switching of aluminum oxide for flexible memory devices. *Appl. Phys. Lett.* **2009**, *92*, 223508.
(35) Wu, Y.; Lee, B.; Wong, H.-S. P. Al_2O_3-based RRAM using atomic layer deposition (ALD) with 1μA reset current. *IEEE Electron Device Lett.* **2010**, *31*, 1449.
(36) Yao, J.; Sun, Z.; Zhong, L.; Natelson, D.; Tour, J. M. Resistive switches and memories from silicon oxide. *Nano Lett.* **2010**, *10*, 4105.
(37) Jung, K.; Kim, Y.; Park, Y. S.; Jung, W.; Choi, J.; Park, B.; Kim, H.; Kim, W.; Hong, J.; Im, H. Unipolar resistive switching in insulating niobium oxide and probing electroforming induced metallic components. *J. Appl. Phys.* **2011**, *109*, 054511.
(38) Choi, S.-J.; Lee, J.-H.; Bae, H.-J.; Yang, W.-Y.; Kim, T.-W.; Kim, K.-H. Improvement of CBRAM resistance window by scaling down electrode size in pure-GeTe film. *IEEE Electron Device Lett.* **2009**, *30*, 120.
(39) Do, Y. H.; Jeong, K. W.; Kim, C. O.; Hong, J. P. Electroforming and switching properties of Binary-Oxide TiO_2 thin films for nonvolatile memory applications. *J. Korean Phys. Soc.* **2006**, *48*, 1492.
(40) Terabe, K.; Hasegawa, T.; Nakayama, T.; Aono, M. Quantized conductance atomic switch. *Nature* **2005**, *433*, 47–50.
(41) Yang, Y. C.; Pan, F.; Liu, Q.; Liu, M.; Zeng, F. Fully room-temperature-fabricated nonvolatile resistive memory for ultrafast and high-density memory application. *Nano Lett.* **2009**, *9*, 1636.
(42) Lee, C.; Kim, I.; Shin, H.; Kim, S.; Cho, J. Nonvolatile resistive switching memory properties of thermally annealed titania precursor/polyelectrolyte multilayers. *Langmuir* **2009**, *25*, 11276.
(43) Kim, D. C.; Seo, S.; Ahn, S. E.; Suh, D.-S.; Lee, M. J.; Park, B.-H.; Yoo, I. K.; Baek, I. G.; Kim, H.-J.; Yim, E. K.; Lee, J. E.; Park, S. O.; Kim, H. S.; Chung, U-In; Moon, J. T.; Ryu, B. I. Electrical observations of filamentary conductions for the resistive memory switching in NiO films. *Appl. Phys. Lett.* **2006**, *88*, 202102.
(44) Choi, B. J.; Jeong, D. S.; Kim, S. K.; Rohde, C.; Choi, S.; Oh, J. H.; Kim, H. J.; Hwang, C. S.; Szot, K.; Waser, R.; Reichenberg, B.; Tiedke, S. Resistive switching mechanism of TiO_2 thin films grown by atomic-layer deposition. *J. Appl. Phys.* **2005**, *98*, 033715.
(45) Mao, Q.; Ji, Z.; Xi, J. Realization of forming-free Zn-based resistive switching memory by controlling film thickness. *J. Phys. D: Appl. Phys.* **2010**, *43*, 395104.
(46) Kang, Y. H.; Choi, J.-H.; Lee, T. I.; Lee, W.; Myoung, J.-M. Thickness dependence of the resistive switching behavior of nonvolatile memory device structures based on undoped ZnO films. *Solid State Commun.* **2011**, *151*, 1739.
(47) Yang, J. J.; Strachan, J. P.; Xia, Q.; Ohlberg, D. A. A.; Kuekes, P. J.; Kelley, R. D.; Stickle, W. F.; Stewart, D. R.; Medeiros-Ribeiro, G.; Williams, R. S. Diffusion of adhesion layer metals controls nanoscale memristive switching. *Adv. Mater.* **2010**, *22*, 4034.